Theoretical Kinetics Analysis for Ḣ Atom Addition to 1,3-Butadiene and Related Reactions on the $\dot{C}_4H_7$ Potential Energy Surface

Yang Li [1], Stephen J. Klippenstein[2], Chong-Wen Zhou[3], Henry J. Curran[*,1]

[1]Combustion Chemistry Centre, National University of Ireland, Galway, Ireland

[2]Chemical Sciences and Engineering Division, Argonne National Laboratory, 9700 S. Cass Ave., Argonne, IL 60439, USA

[3]School of Energy and Power Engineering, Beihang University, Beijing 100191, P. R. China.

Abstract

The oxidation chemistry of the simplest conjugated hydrocarbon, 1,3-butadiene, can provide a first step in understanding the role of poly-unsaturated hydrocarbons in combustion and, in particular, an understanding of their contribution towards soot formation. Based on our previous work on propene and the butene isomers (1-, 2- and isobutene), it was found that the reaction kinetics of H-atom addition to the C=C double bond plays a significant role in fuel consumption kinetics and influences the predictions of high-temperature ignition delay times, product species concentrations and flame speed measurements. In this study, the rate constants and thermodynamic properties for Ḣ-atom addition to 1,3-butadiene and related reactions on the $\dot{C}_4H_7$ potential energy surface have been calculated using two different series of quantum chemical methods and two different kinetic codes. Excellent agreement is obtained between the two different kinetics codes. The calculated results including zero point energies, single point energies, rate constants, barrier heights and thermochemistry are systematically compared among the two quantum chemical methods. 1-methylallyl ($\dot{C}_4H_7$1-3) and 3-buten-1-yl ($\dot{C}_4H_7$1-4) radicals and C_2H_4 + $\dot{C}_2H_3$ are found to be the most important channels and reactivity promoting products, respectively. We calculated that terminal addition is dominant (> 80%) compared to internal Ḣ-atom addition at all temperatures in the range 298 – 2000 K. However, this dominance decreases with increasing temperature. The calculated rate constants for the bimolecular reaction C_4H_6 + Ḣ → products and C_2H_4 + $\dot{C}_2H_3$ → products are in excellent agreement with both experimental and theoretical results from the literature. For selected C_4 species the calculated thermochemical values are also in good agreement with literature data. In addition, the rate constants for H-atom abstraction by Ḣ atoms have also been calculated, and it is found that abstraction from the central carbon atoms is the dominant channel (> 70%) at temperatures in the range 298 – 2000 K. Finally, by incorporating our calculated rate constants for both H-atom addition and abstraction into our recently developed 1,3-butadiene model, we show that laminar flame speed predictions are significantly improved, emphasizing the value of this study.

* Corresponding author: henry.curran@nuigalway.ie

1. Introduction

In our recent mechanism development studies for propene,[1-2] 1-butene,[3] 2-butene,[4] isobutene,[5] and 1,3-butadiene[6] oxidation, the reaction kinetics for Ḣ-atom addition to the C=C double bond was found to be critical in predicting high-temperature ignition delay times, speciation and flame speeds. For the 1-methylallyl ($\dot{C}_4H_7$1-3) radical, which is a key intermediate in 1,3-butadiene oxidation, isomerization, Ḣ-atom elimination and β-scission reactions are the major consumption pathways at high temperatures (> 1100 K). Over the past thirty years, there have been a number of modeling, theoretical and experimental studies of 1,3-butadiene oxidation. For example, Laskin *et al.*[7] studied the kinetics of 1,3-butadiene oxidation over the 1035–1185 K temperature regime using a detailed kinetic model. They found that the chemically activated reaction of Ḣ atom with 1,3-butadiene to produce ethylene and vinyl radical is the most important channel at all of their experimental conditions. These observations point to the importance of understanding the kinetics of reactions on the $\dot{C}_4H_7$ potential energy surface (PES).

Reactions on the $\dot{C}_4H_7$ PES have been the subject of a number of prior theoretical studies. Miller *et al.*[8] used the G3//B3LYP quantum chemical method to calculate the geometries, vibrational frequencies, and energies of five $\dot{C}_4H_7$ radical isomers and transition states for the corresponding dissociation and isomerization reactions on the $\dot{C}_4H_7$ PES. Miyoshi *et al.*[9] reported CBS-QB3 based *ab initio* Rice Ramsperger Kassel Marcus (RRKM) and master equation (ME) calculations of the reaction kinetics for 3-butenyl and 3-butenylperoxy radicals. Xu *et al.*[10] performed a series of CBS-QB3 based quantum RRK/modified strong collider analyses for the reactions on the $\dot{C}_3H_7$, $\dot{C}_4H_7$, and $\dot{C}_4H_9$ potential energy surfaces in order to characterize the radical addition reactions that lead to molecular weight growth. Most recently, Huang *et al.*[11] explored the complete $\dot{C}_4H_7$ PES at the CCSD(T)-F12/cc-pVTZ-F12//QCISD/6-311++G(2df,2p) level, including both straight-chain and branched backbones. They also explored the kinetics with RRKM/ME calculations covering the range from 800 to 2500 K and 0.01 to 100 atm. Their calculations indicate that the transformation from *i*-$\dot{C}_4H_7$ to the straight-chain $\dot{C}_4H_7$ radical is kinetically unfavorable due to the high strain energy of the 3-membered ring structure in the transition state.

Shestov *et al.*[12] investigated the bimolecular reaction C_2H_4 + $\dot{C}_2H_3$ using the laser photolysis/photoionization mass spectrometry technique in the temperature range 625 – 950 K and bath gas (helium) densities of (6 – 12) × 10^{16} atom cm^{-3}. C_4H_6 and $\dot{C}_4H_7$ were detected as the primary products, and the thermal stability of the $\dot{C}_4H_7$ radical at 950 K indicated that it is a delocalized radical. The observed total reaction rate constant was represented by the expression $k_1 = 10^{-11.69 \pm 0.44}$ exp(–2830 ± 790 K/*T*) cm^3 $molecule^{-1}$ s^{-1}.

Ismail *et al.*[13] reported direct measurements of absolute rate coefficients for the $\dot{C}_2H_3$ + C_2H_4 reaction over the temperature range 300 – 700 K and at 20 and 133 mbar. The measured results at a pressure of 20 mbar were in good agreement with previous determinations for the $\dot{C}_2H_3$ + C_2H_4 bimolecular reaction at higher temperatures (600–750 K). At a pressure of 133 mbar, the observed rate constants were fit to a modified three-parameter Arrhenius expression: $k = (7 \pm 1) \times 10^{-14}$ $(T/298\ K)^2$ exp[–(1430 ± 70) K/*T*] cm^3 $molecule^{-1}$ s^{-1}.

The objectives of the current study are to calculate the thermodynamic properties and rate coefficients for Ḣ-atom addition to 1,3-butadiene and its related reactions on the $\dot{C}_4H_7$ PES using *ab initio* TST methods. Moreover, comprehensive comparisons are carried out between (i) two different series of *ab initio* methods, (ii) two different kinetic program codes, namely, MultiWell[14] and PAPR[15] and (iii) calculated results and experimental data in the literature.

2. Theoretical and Computational Approach

In this study, two different series of *ab initio* electronic structure methods have been applied using Gaussian 09[16] as summarized in Table 1.

Table 1: Quantum chemical methods used for rate coefficient and thermochemistry calculations.

	Method 1	Method 2
Geometry & Frequency	M06-2X/6-311++G(d,p)	wB97XD/aug-cc-pVTZ
Scan & IRC	M06-2X/6-311++G(d,p)	
Electronic Energy	–	CCSD(T)/aug-cc-pVTZ
	CCSD(T)/cc-pVTZ	MP2/aug-cc-pVTZ
	CCSD(T)/cc-pVQZ	MP2/aug-cc-pVQZ
Zero Kelvin Energy	CBS-APNO/G3/G4	

In the first series of calculations, the M06-2X[17] method with the 6-311++G(d,p)[18-19] basis set was used for the geometry optimizations, vibrational frequency calculations and also the hindered rotation treatments for lower frequency modes. All vibrational frequencies and zero point vibrational energies (ZPVEs) were scaled by 0.983 and 0.9698 respectively, which was recommended for the M06-2X functional by Zhao and Truhlar.[17] The electronic single point energies (SPEs) were calculated at the CCSD(T)/cc-pVXZ level of theory (where X = T and Q),[20-21] and the resulting SPEs were extrapolated to the complete basis set (CBS) limit using the following formula:[22-23]

$$E_{CBS} = E_{CCSD(T)/cc-pVQZ} + (E_{CCSD(T)/cc-pVQZ} - E_{CCSD(T)/cc-pVTZ}) * 4^4/(5^4 - 4^4)$$

In the second series, the geometry optimizations and frequency calculations were carried out at the wB97XD/aug-cc-pVTZ[24-26] level of theory. Meanwhile, single point energies were obtained from a combination of CCSD(T)/aug-cc-pVTZ, MP2/aug-cc-pVTZ and MP2/aug-cc-pVQZ[27] calculations:

$$E_{CBS} = (E_{MP2/aug-cc-pVQZ} - E_{MP2/aug-cc-pVTZ}) + E_{CCSD(T)/aug-cc-pVTZ}$$

In both quantum chemical methods, internal rotations that correspond to low frequency torsional modes were scanned in 10 degree increments as a function of dihedral angle using the M06-2X/6-311++G(d,p) method. This method was also used to perform intrinsic reaction coordinate (IRC) calculations[28] on each transition state (TS) to ensure it was connected to the desired reactants and products. The T_1 diagnostic[29] for

all reactant species is ≤ 0.025, which indicates the reliability of single-reference methods for describing the wave function. T_1 values for all the TSs are ≤ 0.044. Klippenstein *et al.* [30] mentioned that T_1 values of radical species that greater than 0.03 become a cause for concern. On this $\dot{C}_4H_7$ PES, only five of the twenty-three complexes have T_1 values greater than 0.035. For those few cases, either multi-reference or higher-order coupled cluster calculations would be recommended for higher accuracies.

For the MultiWell[14] program suite calculation, the Lamm module was used to calculate both external rotational constants and reduced moment of inertia for the hindered internal rotations. The calculated results were then fitted to truncated Fourier series, which were further used as 1-D hindered internal rotation input in the Thermo module. The high-pressure limit (HPL) rate coefficients were finally calculated by the Thermo module as a function of temperature (298.15 – 2000 K) based on canonical transition state theory (TST).[31]

In the PAPR[15] program suite calculation, the Master Equation System Solver (MESS) was used to calculate temperature and pressure dependent rate coefficients for complex-forming reactions via solution of the one-dimensional ME, with the chemical transformations described using RRKM theory.[32-36] Rate coefficients for the thermally and chemically activated reactions are obtained at temperatures ranging from 298.15 to 2000 K, and at pressures ranging from 0.01 to 100 atm. The internal rotors corresponding to methyl and ethyl like torsions were treated as 1-dimensional hindered rotors with hindrance potentials evaluated at the M06-2X/6-311++G(d,p) level of theory. However, the reduced moment of inertia is calculated based on the structure of the most stable species, the axis of rotation, and the identity of all the atoms on each side of the rotated bond. Although an algorithm that properly treats the internal rotation variation of both the internal and external rotational constants is available in MESS, for simplicity we assumed that the internal and external moments of inertia are constant, i.e., not a function of the dihedral angle. Note that this assumption is justified by the fact that the neglect of the coupling of external and internal rotation often counterbalances the neglect of the dihedral angle variance of the internal rotor moment of inertia. For the collisional model used in the master equation simulation, the interaction between the reactant and N_2 bath gas was modeled using the Lennard–Jones (L–J) potential.[37] The L–J parameters were calculated by the method described in.[38] For N_2, σ = 3.6 Å and ε = 68 cm^{-1} were used, while for $\dot{C}_4H_7$, σ = 4.5 Å and ε = 1450 cm^{-1} were used. The collisional energy transfer function was represented by a single-parameter exponential down model with $\langle\Delta E\rangle_{down} = 200 \times (T/300)^{0.75}$ cm^{-1}, which has served as a fairly good model for C_3, C_4 hydrocarbons.[9, 39-40]

In both program suites, quantum mechanical tunneling was taken into account for an unsymmetrical Eckart barrier model.[41] The calculated rate coefficients were fitted to a modified Arrhenius expression as a function of temperature:

$$k = \mathrm{A}\left(T/T_{ref}\right)^{\mathrm{n}}\exp(-E/RT)$$

Where A is the A-factor, T is the temperature in units of Kelvin, T_{ref} = 1 K, n is the temperature exponent at 1 K, and E is related to the activation energy (by $Ea = E + nRT$).

As to the quantum chemical methods for the thermodynamic properties calculation, the average atomization formation enthalpies for all of the C_4 species on the $\dot{C}_4H_7$ PES were carried out using a combined

compound method CBS-APNO/G3/G4,[42-44] which was found to yield results approaching "chemical accuracy" (arbitrarily, ≈ 4 kJ mol^{-1} or 1 kcal mol^{-1}) when benchmarked against enthalpy of formation values in the Active Thermochemical Tables (ATcT).[45-47] The thermochemical values of interest (enthalpy of formation, entropy and heat capacity) were calculated as a function of temperature (298.15−3000 K), and these resulting values were fitted to NASA polynomials[48] using the Fitdat utility in ANSYS CHEMKIN-PRO.[49]

3. Results and Discussion

3.1. $\dot{C}_4H_7$ Potential Energy Surface

The results of the electronic structure calculations for the association, dissociation and isomerization pathways are depicted in Fig. 1, which contains 19 species and 23 transition states. These relative energies (with ZPE corrections included) were calculated using Method 1, as outlined in Table 1, and all isomerization (red lines) and dissociation (blue lines) reaction pathways are highlighted. Note, for all the C_4H_6 and C_4H_7 species in this paper, we focus on the trans-structure, although the cis-structures are generally included implicitly in the kinetic analysis through torsional treatments.

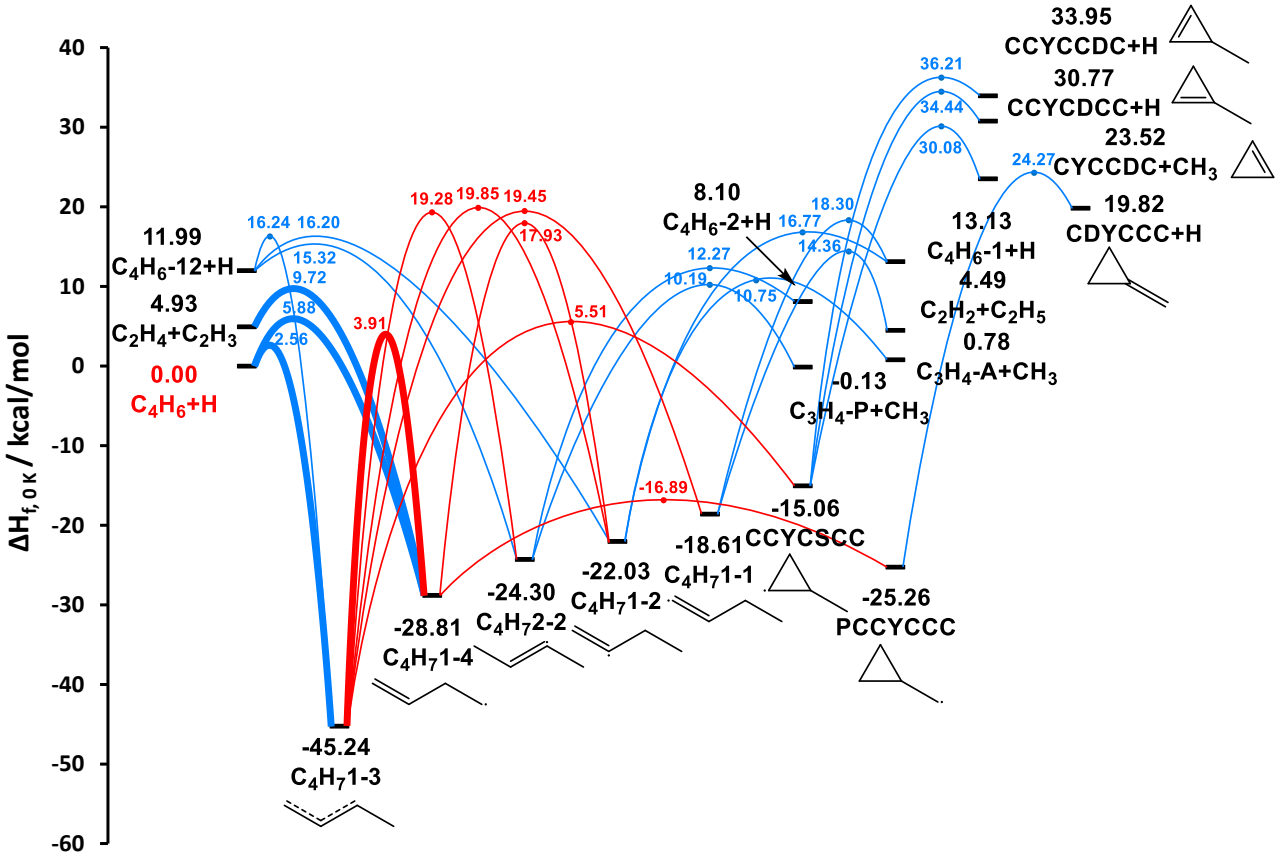

Fig. 1. $\dot{C}_4H_7$ Potential Energy Surface.

For the reaction of Ḣ atoms with 1,3-butadiene, Ḣ atoms can add to either the terminal carbon atom to form 1-methylallyl ($\dot{C}_4H_7$1-3) radical or to the central carbon to form 3-buten-1-yl ($\dot{C}_4H_7$1-4) radical. The barrier for terminal addition is 3.32 kcal mol^{-1} lower than that for central addition, while the barrier for isomerization between these two radicals lies between the two entrance barriers. Obviously, these two entrance wells are found to be the most important wells on the $\dot{C}_4H_7$ PES. 1-methylallyl ($\dot{C}_4H_7$1-3) radical has

the lowest energy among all of the wells. Meanwhile, 3-buten-1-yl ($\dot{C}_4H_7$1-4) radical is the most "reactivity promoting" well, leading to the formation of ethylene and vinyl radicals via β-scission.

As shown in Fig. 1, the 1-methylallyl ($\dot{C}_4H_7$1-3) and 3-buten-1-yl ($\dot{C}_4H_7$1-4) radicals can isomerize to form the other three straight-chain and two cyclic structural $\dot{C}_4H_7$ isomers: 2-buten-2-yl ($\dot{C}_4H_7$2-2), 1-buten-2-yl ($\dot{C}_4H_7$1-2), 1-buten-1-yl ($\dot{C}_4H_7$1-1), 2-methylcyclopropyl (CCYCSCC) and cyclo-propyl-methyl (PCCYCCC) radicals. All of these wells can then dissociate via β-scission reactions. For the most part, the isomerization barriers are significantly higher than those of dissociation reactions. In addition, the TSs for the isomerization reactions are much tighter than those for the dissociations. Therefore, most of the isomerization reactions are not competitive with the dissociation reactions.

The energies (relative to C_4H_6 + Ḣ) of all of the species and transition states (TSs) on the $\dot{C}_4H_7$ PES have also been calculated using Method 2, and are compared to those from Method 1, from ATcT,[45-47] and from Huang et al.[11] in Table 2 and Table 3. The calculated energies for the two present quantum chemistry methods are all within 0.4 kcal mol^{-1}, demonstrating the internal consistency of the two methods. The CCSD(T)-F12/cc-pVTZ-F12//QCISD/6-311++G(2df,2p) results of Huang et al. are also quite similar, although differences of as much as 1.7 kcal/mol are observed.

Table 2: Comparison of the calculated relative energies (Δ_fH_{0K}) (kcal mol^{-1}) for all species on the $\dot{C}_4H_7$ PES.

	Method 1	Method 2	ATcT[45-47]	Huang *et al.* [11]
		Reactants		
C_4H_6 + Ḣ	0.00	0.00	0.00	0.00
		Wells		
$\dot{C}_4H_7$1-3	–45.24	–44.93	–	–45.1
$\dot{C}_4H_7$1-4	–28.81	–28.79	–	–28.1
$\dot{C}_4H_7$2-2	–24.30	–24.19	–	–
$\dot{C}_4H_7$1-2	–22.03	–21.99	–	–21.7
$\dot{C}_4H_7$1-1	–18.61	–18.65	–	–
CCYCSCC	–15.06	–15.15	–	–14.3
PCCYCCC	–25.26	–25.26	–	–24.8
		Products		
C_4H_6-12 + Ḣ	11.99	11.93	–	13.4
C_2H_4 + $\dot{C}_2H_3$	4.93	4.80	5.02	4.8
C_4H_6-2 + Ḣ	8.10	8.17	8.10	–
C_3H_4-p + $\dot{C}H_3$	–0.13	–0.27	0.36	–
C_4H_6-1 + Ḣ	13.13	13.03	12.98	12.2
C_3H_4-a + $\dot{C}H_3$	0.78	0.66	1.44	1.2
$\dot{C}_2H_5$ + C_2H_2	4.49	4.26	4.46	–
CCYCCDC + Ḣ	33.95	33.78	–	–
CCYCDCC + Ḣ	30.77	30.68	–	–
CYCCDC + $\dot{C}H_3$	23.52	23.30	24.20	–
CDCYCCC + Ḣ	19.82	19.75	–	–

Table 3: Comparison of the calculated relative energies ($\Delta_f H_{0K}$) (kcal mol^{-1}) for all TSs on the $\dot{C}_4H_7$ PES.

	Method 1	Method 2	Huang *et al.* [11]
TSs for Isomerization Reactions			
$\dot{C}_4H_7$1-3 ↔ $\dot{C}_4H_7$1-4	3.91	4.02	3.9
$\dot{C}_4H_7$1-3 ↔ $\dot{C}_4H_7$2-2	19.28	19.30	–
$\dot{C}_4H_7$1-3 ↔ $\dot{C}_4H_7$1-2	19.85	19.85	20.2
$\dot{C}_4H_7$1-3 ↔ $\dot{C}_4H_7$1-1	19.45	19.57	–
$\dot{C}_4H_7$1-4 ↔ $\dot{C}_4H_7$1-2	17.93	17.95	17.8
$\dot{C}_4H_7$1-3 ↔ CCYCSCC	5.51	5.53	5.2
$\dot{C}_4H_7$1-4 ↔ PCCYCCC	–16.89	–16.86	–16.8
TSs for Dissociation Reactions			
$\dot{C}_4H_7$1-3 ↔ C_4H_6-12 + $\dot{H}$	16.24	16.06	–
$\dot{C}_4H_7$1-3 ↔ C_4H_6 + $\dot{H}$	2.56	2.54	1.7
$\dot{C}_4H_7$1-4 ↔ C_2H_4 + $\dot{C}_2H_3$	9.72	9.69	8.8
$\dot{C}_4H_7$1-4 ↔ C_4H_6 + $\dot{H}$	5.88	5.85	5.1
$\dot{C}_4H_7$2-2 ↔ C_4H_6-2 + $\dot{H}$	12.27	12.10	–
$\dot{C}_4H_7$2-2 ↔ C_4H_6-12 + $\dot{H}$	15.32	15.18	–
$\dot{C}_4H_7$2-2 ↔ C_3H_4-p + $\dot{C}H_3$	10.19	9.91	–
$\dot{C}_4H_7$1-2 ↔ C_4H_6-1 + $\dot{H}$	16.77	16.48	16.8
$\dot{C}_4H_7$1-2 ↔ C_4H_6-12 + $\dot{H}$	16.20	16.04	17.8
$\dot{C}_4H_7$1-2 ↔ C_3H_4-a + $\dot{C}H_3$	10.75	10.54	11.9
$\dot{C}_4H_7$1-1 ↔ C_4H_6-1 + $\dot{H}$	18.30	17.96	–
$\dot{C}_4H_7$1-1 ↔ C_2H_2 + $\dot{C}_2H_5$	14.36	14.02	–
CCYCSCC ↔ CCYCCDC + $\dot{H}$	36.21	35.94	–
CCYCSCC ↔ CCYCDCC + $\dot{H}$	34.44	34.23	–
CCYCSCC ↔ CYCCDC + $\dot{C}H_3$	30.08	29.69	–
PCCYCCC ↔ CDCYCCC + $\dot{H}$	24.27	24.04	–

3.2. Barrier Height Comparison

Ibukl *et al.*[50] obtained the threshold energy of 33.0 kcal mol^{-1} for the 1,2-H atom shift from 3-buten-1-yl ($\dot{C}_4H_7$1-4) radical to 1-methylallyl ($\dot{C}_4H_7$1-3) radical. Miller *et al.*[51] investigated the unimolecular reaction dynamics of 1-buten-2-yl ($\dot{C}_4H_7$1-2) radicals using a molecular beam scattering technique. They found that with at least 30.7 ± 2 kcal mol^{-1} of internal energy, this radical underwent C–C fission to form allene and methyl radicals, and with at least 36.7 ± 4 kcal mol^{-1} of internal energy it underwent C–H fission to form $\dot{H}$ atoms and either 1-butyne or 1,2-butadiene. McCunn *et al.*[52] studied the unimolecular dissociation of the 2-buten-2-yl ($\dot{C}_4H_7$2-2) radical using a crossed laser-molecular beam technique. They found that the lowest-energy dissociation barrier of C–C bond fission was 31 ± 2 kcal mol^{-1}, and that there was a 7.5 ± 2 kcal mol^{-1} energy barrier for the reverse bimolecular reaction of methyl radicals with propyne.

In Table 4, the barrier heights calculated here are compared with the experimental data discussed above. Firstly, the barriers calculated by the two quantum chemical methods are in good agreement, which are consistently within 0.4 kcal mol^{-1} of one another. Secondly, the calculated results agree well with the experimental data, which indicates the reliability of both methods in terms of energy calculations.

Table 4: Barrier heights for the dissociation reactions from 1-buten-1-yl ($\dot{C}_4H_7$1-1), 1-buten-2-yl ($\dot{C}_4H_7$1-2) and 2-buten-2-yl ($\dot{C}_4H_7$2-2) wells.

Reactions	Experiment	Method 1	Method 2
$\dot{C}_4H_7$1-4 ↔ $\dot{C}_4H_7$1-3	33.0	32.7	32.8
$\dot{C}_4H_7$1-2 ↔ C_3H_4-a + $\dot{C}H_3$	≤ 30.7 ± 2	32.8	32.5
$\dot{C}_4H_7$1-2 ↔ C_4H_6-12 + $\dot{H}$	≤ 36.7 ± 4	38.8	38.5
$\dot{C}_4H_7$1-2 ↔ C_4H_6-1 + $\dot{H}$	≤ 36.7 ± 4	38.2	38.0
$\dot{C}_4H_7$2-2 ↔ C_3H_4-p + $\dot{C}H_3$	≤ 31.0 ± 2	34.5	34.1
C_3H_4-p + $\dot{C}H_3$ ↔ $\dot{C}_4H_7$2-2	≤ 7.5 ± 2	10.3	10.2

3.3. Comparison of HPL Rate Constants between Two Different Quantum Chemical Methods and Codes

The HPL rate constants calculated by the two different quantum chemical methods for the thermal decomposition and isomerization reactions on the $\dot{C}_4H_7$ PES are illustrated in Fig. 2a – 2h. The different colors used there correspond to different reactions from each well, while solid and dashed lines correspond to the results calculated from the first and second methods, respectively. At combustion temperatures (600 – 2000 K), the rate constants calculated using the first quantum chemical method are consistently smaller than those calculated using the second, however, the differences are within 50% of one another. This finding is consistent with the slightly higher (0.1 – 0.5 kcal mol^{-1}) barrier heights predicted by the first method. The small magnitude of the difference suggests that the computationally much cheaper second method still yields reasonably accurate kinetic results. All of these HPL rate constants have been fitted in a modified Arrhenius form, and are provided as Supplementary Material.

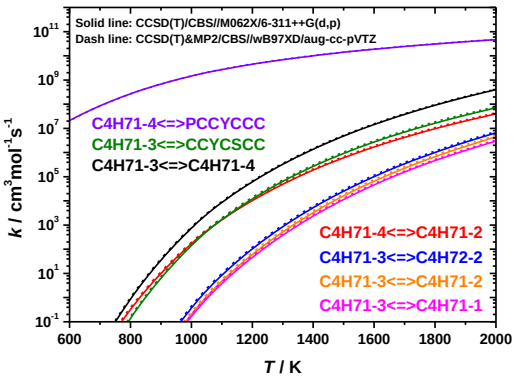

(a) isomerization reactions for all C_4H_7 wells

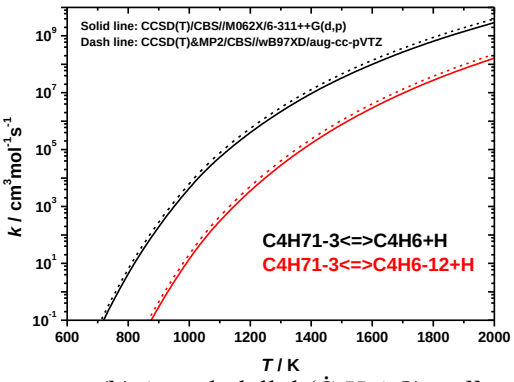

(b) 1-methylallyl ($\dot{C}_4H_7$1-3) well

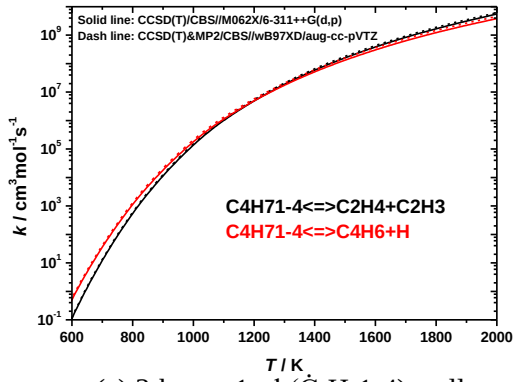

(c) 3-buten-1-yl ($\dot{C}_4H_7$1-4) well

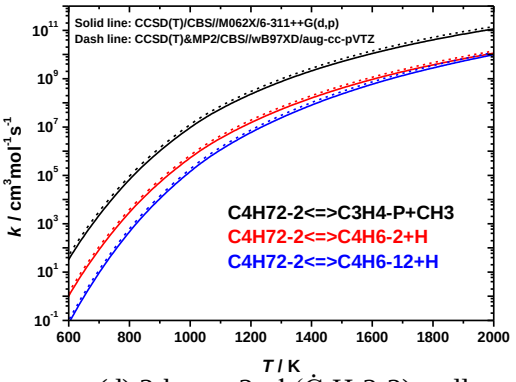

(d) 2-buten-2-yl ($\dot{C}_4H_7$2-2) well

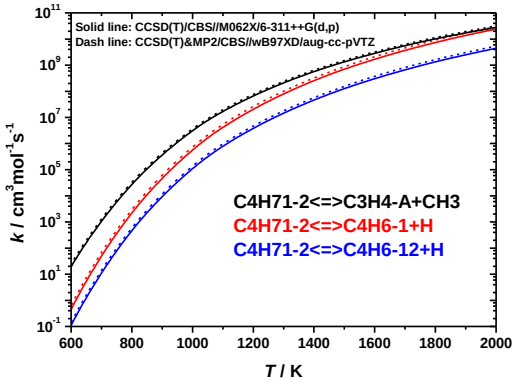

(e) 1-buten-2-yl ($\dot{C}_4H_7$1-2) well

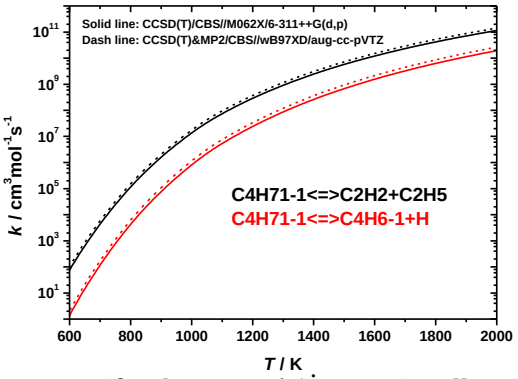

(f) 1-buten-1-yl ($\dot{C}_4H_7$1-1) well

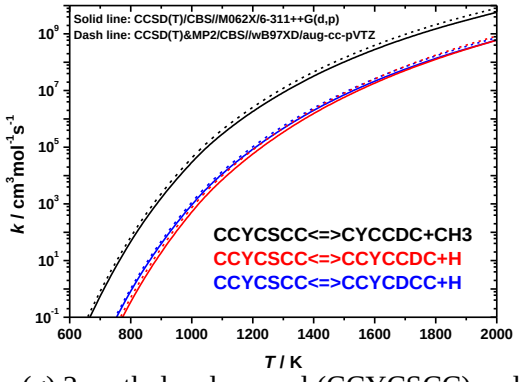

(g) 2-methylcyclopropyl (CCYCSCC) well

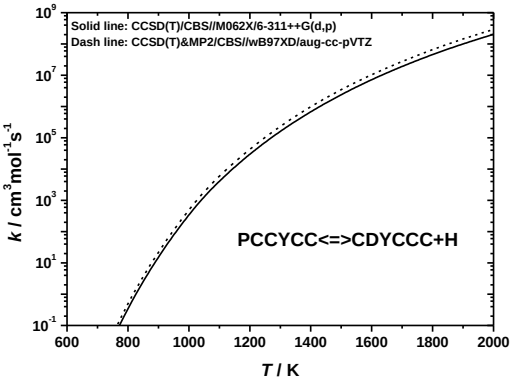

(h) cyclopropylmethyl (PCCYCCC) well

Fig. 2. HPL rate constants for the isomerization and thermal decomposition reactions on the $\dot{C}_4H_7$ PES calculated by two quantum chemical methods. Solid lines: Method 1; dash lines: Method 2.

In order to compare the performance of the two kinetic codes, the HPL rate constants for terminal and central Ḣ-atom addition to 1,3-butadiene were calculated and their branching ratios compared over the

temperature range 600–2000 K, Table 5. Notably, for both terminal and central atom addition, the rate constants calculated using MultiWell/Thermo and PAPR are in excellent agreement, being within 3% of one another over the entire temperature range. Furthermore, the calculated branching ratio (terminal addition to central addition) demonstrates that terminal addition dominates, with this dominance decreasing slightly with increasing temperature.

Table 5: Comparison of the predicted HPL rate constants for terminal and central Ḣ atom addition reactions calculated using two codes.

	MultiWell/Thermo			PAPR		
T / K	Terminal addition	Central addition	Branching ratio	Terminal addition	Central addition	Branching ratio
600	8.96E+12	4.18E+11	96 : 4	8.72E+12	4.09E+11	96 : 4
800	1.99E+13	1.67E+12	92 : 8	1.94E+13	1.64E+12	92 : 8
1000	3.47E+13	4.13E+12	89 : 11	3.37E+13	4.05E+12	89 : 11
1100	4.34E+13	5.86E+12	88 : 12	4.22E+13	5.74E+12	88 : 12
1200	5.29E+13	7.91E+12	87 : 13	5.15E+13	7.76E+12	87 : 13
1300	6.32E+13	1.03E+13	86 : 14	6.15E+13	1.01E+13	86 : 14
1400	7.42E+13	1.30E+13	85 : 15	7.22E+13	1.28E+13	85 : 15
1500	8.59E+13	1.60E+13	84 : 16	8.36E+13	1.57E+13	84 : 16
1600	9.84E+13	1.93E+13	84 : 16	9.57E+13	1.90E+13	83 : 17
1700	1.11E+14	2.29E+13	83 : 17	1.08E+14	2.26E+13	83 : 17
1800	1.25E+14	2.69E+13	82 : 18	1.22E+14	2.64E+13	82 : 18
1900	1.39E+14	3.10E+13	82 : 18	1.36E+14	3.06E+13	82 : 18
2000	1.54E+14	3.55E+13	81 : 19	1.50E+14	3.50E+13	81 : 19

3.4. Rate Constants Comparison Against Experimental and Theoretical Results in Literature

3.4.1. C_4H_6 + Ḣ Bimolecular Reaction

There have been a number of experimental investigations on the kinetics of the C_4H_6 + Ḣ bimolecular reaction, Table 6. Most of these investigations are limited to low temperatures, pressure and are not product specific. Fig. 3 provides a comparison of our calculation results with previously measured[53-61] and computed[11] rate coefficients for C_4H_6 + Ḣ → products. Our calculations are in excellent agreement with the experimental measurements. Moreover, the high pressure limit (HPL), terminal addition, central addition, and chemically activated reaction rate constants are also in good agreement with the theoretical results from Huang *et al.*[11], which ultimately suggests the reliability of the quantum chemical and kinetics methods applied in this study and in that by Huang *et al*.

Table 6: Literature experimental data for the C_4H_6 + Ḣ reaction rate constant.

Temperature / K	Pressure / Torr	Reference
296.5	435	Jennings *et al.* 1961 [53]
296.5	501	Yang *et al.* 1962 [54]
298	–	Woolley *et al.* 1969 [55]
298	–	Cvetanovic *et al.* 1969 [56]
298	0.38	Koda *et al.* 1971 [57]
298	1.26	Daby *et al.* 1971 [58]
305	–	Gordon *et al.* 1978 [59]
298	500 – 600	Ishikawa *et al.* 1979 [60]
298	50	Oka *et al.* 1979 [61]
1070 – 1120	10	Nametkin *et al.* 1975 [62]

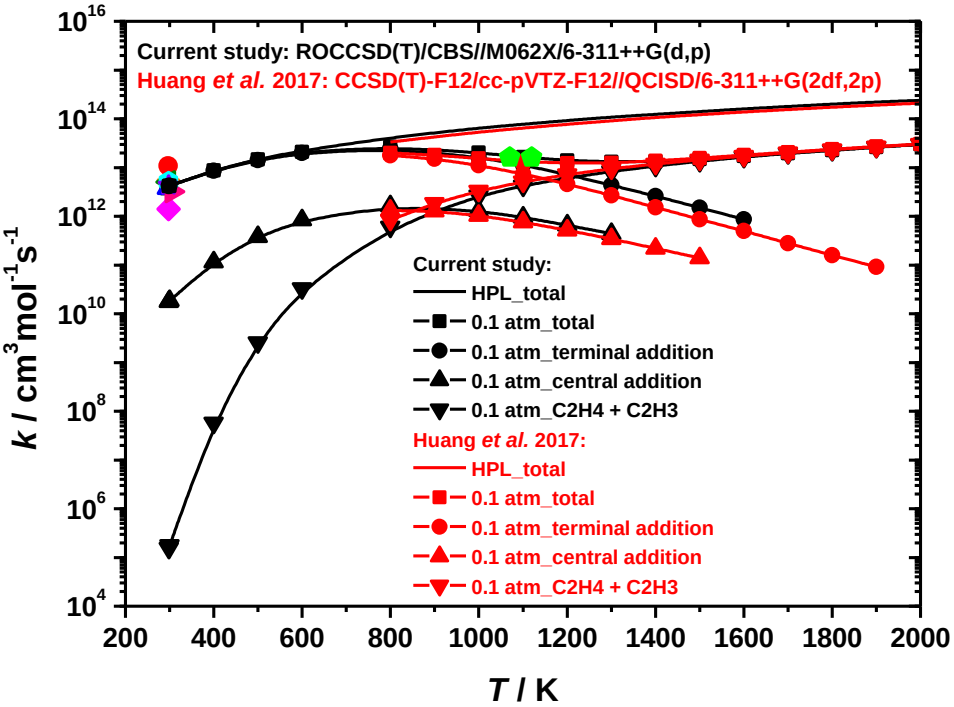

Fig. 3. Theoretical and experimental rate coefficients for C_4H_6 + Ḣ → products. (Experiments: Jennings *et al.* [53], Yang *et al.* [54], Woolley *et al.* [55], Cvetanovic *et al.* [56], Koda *et al.* [57], Daby *et al.* [58], Gordon *et al.* [59], Ishikawa *et al.* [60], Oka *et al.* [61], Nametkin *et al.* [62])

Fig. 4 illustrates the rate coefficients for the reactions associated with the C_4H_6 + Ḣ → products system plotted as a function of temperature at 0.1, 1.0 and 10 atm. Rate coefficients for the three main reaction pathways are illustrated: terminal Ḣ-atom addition forming 1-methylallyl ($\dot{C}_4H_7$1-3) radicals, central Ḣ-atom addition forming 3-buten-1-yl ($\dot{C}_4H_7$1-4) radicals and the chemically activated reaction leading to the formation of ethylene + vinyl radicals. Both the terminal and central addition reactions display a negative temperature dependence at temperatures above about 1100 K, which is enhanced at lower pressure. Both 1-methylallyl ($\dot{C}_4H_7$1-3) and 3-buten-1-yl ($\dot{C}_4H_7$1-4) radicals become thermally unstable with increasing

temperature. On the other hand, the chemically activated reaction shows an obvious negative pressure dependence and reaches its low-pressure limit at about 1700 K. This pathway dominates at higher temperatures and at lower pressures since rapid decomposition due to the excess energy in the chemically activated adduct reduces the yield of stabilized $\dot{C}_4H_7$ radicals. In general, the reaction of 1,3-butadiene with $\dot{H}$ atoms contributes to molecular growth at high pressures and tends to produce bimolecular products that promote chain branching at low pressures.

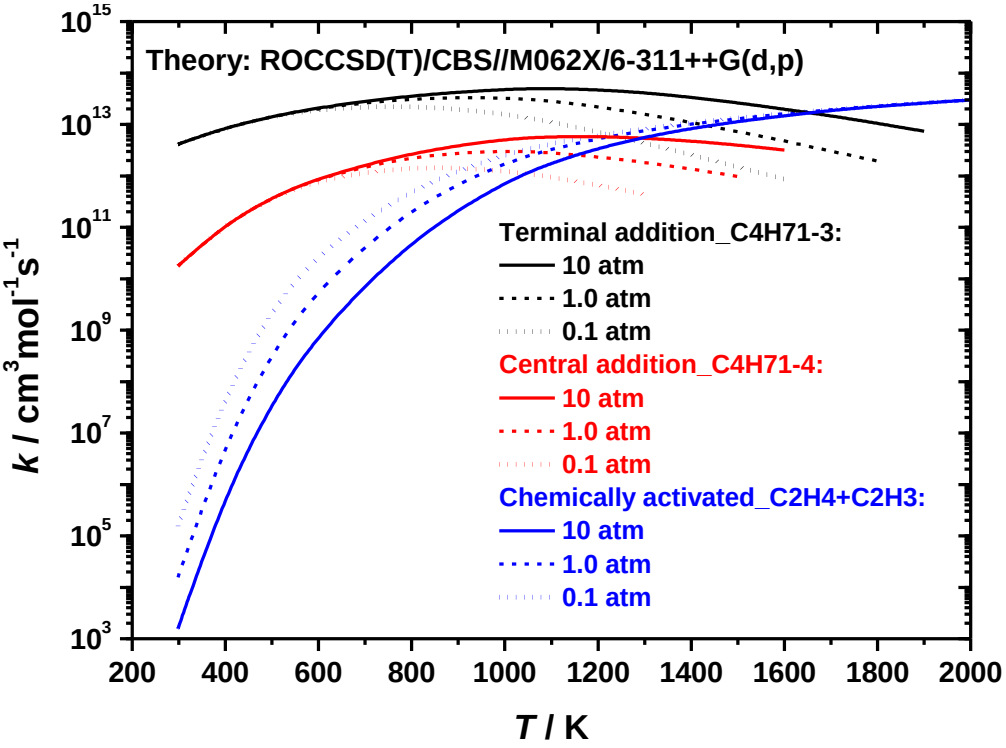

Fig. 4. Pressure dependent rate coefficients for $C_4H_6 + \dot{H} \rightarrow$ products reactions at 0.1, 1.0 and 10 atm.

3.4.2. $C_2H_4 + \dot{C}_2H_3$ Bimolecular Reaction

For the bimolecular reaction $C_2H_4 + \dot{C}_2H_3 \rightarrow$ products, three experimental measurements have been carried out at low pressures from 298 – 1100 K, as shown in Table 7.

Table 7: Experimental kinetic data for $C_2H_4 + \dot{C}_2H_3$ reaction.

Temperature / K	Pressure / mbar	Reference
1023 – 1273	0.0013 – 0.013	Fahr *et al.* 1988[63]
625 – 950	7 – 15	Shestov *et al.* 2005[12]
298 – 700	20 and 133	Ismail *et al.* 2007[13]

As shown in Fig. 5, dissimilar to the $\dot{C}_4H_7$ PES discussed above, ethylene can react with vinyl radicals via a joint cis/trans transition state (B1) to form a joint $\dot{C}_4H_7$1-4 well (W1), followed by the isomerization and dissociation pathways with joint-structure species (W2 and P2) and TSs (B2 – B4). Note, the energies on the PES are the sums of ZPEs and SPEs, and torsional scans of all of the joint-structure species and TSs on the

PES have been performed. Here, we take joint transition state B1 as an example, Fig. 6 shows that trans-structure TS1 and cis-structure TS2 are connected by an internal rotation of the CC–CC dihedral angle, and TS2 is lower in energy than TS1.

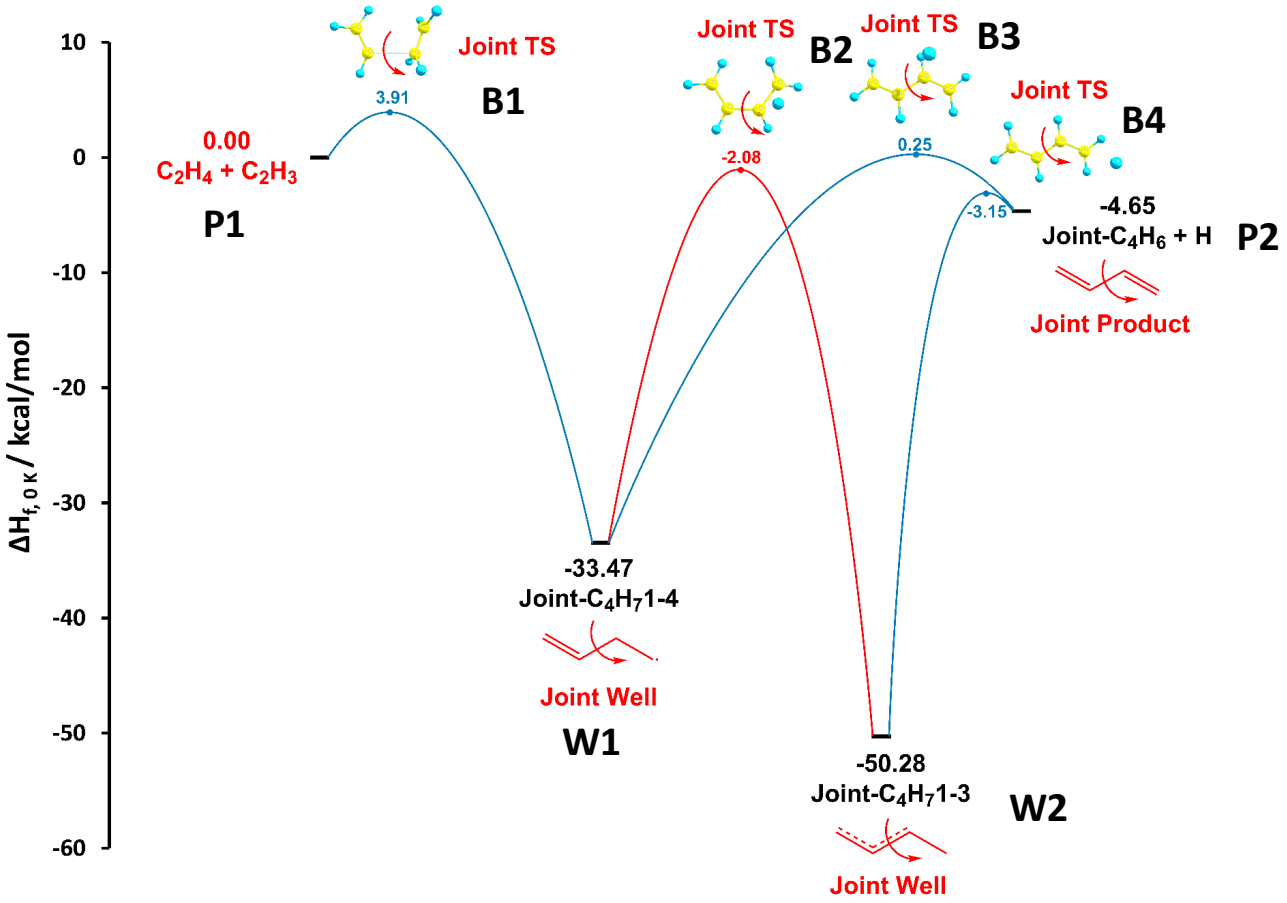

Fig. 5. Complete PES for bimolecular reaction $C_2H_4 + \dot{C}_2H_3 \rightarrow$ products.

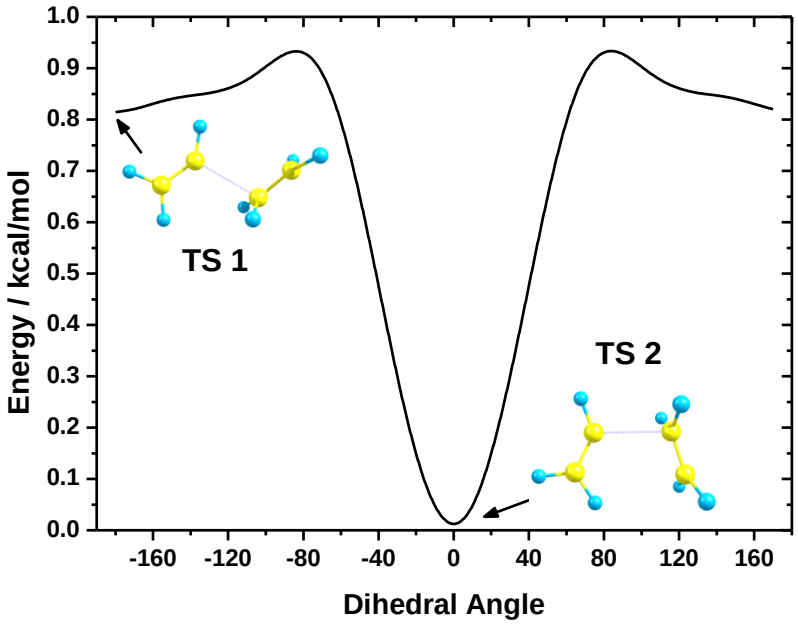

Fig. 6. Internal rotor potential of the CC–CC dihedral angle for the joint transition state B1.

Fig. 7 shows comparisons between theoretical and experimental rate constant calculations/measurements for $C_2H_4 + \dot{C}_2H_3 \rightarrow$ products. The different line colors correspond to the computed rate constants from different sources, with solid and dashed lines representing high-pressure limit rate constants and rate constants at 0.1 atm, respectively. At temperatures in the range 600 – 1100 K, our calculations predict well the experimental results. However, at lower temperature (298 – 600 K), our calculated rate constant is approximately a fact of two smaller than the experimental measurements. Such under prediction reflects 0.5 kcal/mol over prediction of barrier height of the $C_2H_4 + \dot{C}_2H_3$ entrance channel, this probably indicates the need for higher level of electronic structure calculations, with treatment of anharmonic ZPE, core-valence corrections, etc.

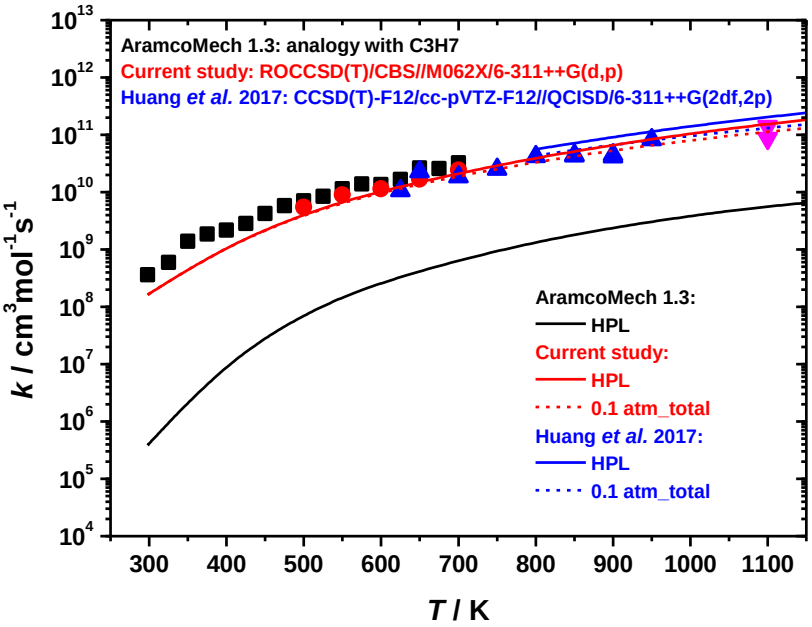

Fig. 7. Comparison between theoretical and experimental rate coefficients for $C_2H_4 + \dot{C}_2H_3 \rightarrow$ products. (Experiments: Fahr *et al.* [63], Shestov *et al.* [12], Ismail *et al.* [13])

3.5. ZPEs and SPEs Evaluation

Zero Point Energies (ZPEs) have been calculated using four different quantum chemical methods for all of the products and transition states associated with the important reaction channels highlighted in Fig. 1. These are as follows:

- Method 1: M06-2X/6-311++G(d,p)
- Method 2: wB97XD/aug-cc-pVTZ
- Method 3: B2PLYP-D3/cc-pVTZ
- Method 4: CCSD(T)/cc-pVTZ

The calculated ZPEs are compared in Table 8, with all energies relative to the $C_4H_6 + \dot{H}$ reactants. The first two methods are those used for all calculations throughout our study, and their values are within 0.2 kcal mol^{-1} of one another, which indicates the consistency of these two methods. The latter two methods were recommended by Klippenstein *et al.*,[64] and the overall comparison of these four methods shows that there is less than 0.7 kcal mol^{-1} difference among them. No value is reported for the 1-methlyallyl ($\dot{C}_4H_7$1-3) radical at

the CCSD(T)/cc-pVTZ level due to symmetry breaking problems that arise due to the resonance stabilization in this radical.

Table 8: Relative ZPE comparison between four different quantum chemical methods.[a] (units: kcal mol^{-1}).

Species & Transition States	Method 1	Method 2	Method 3	Method 4
$C_4H_6 + \dot{H}$	0.00	0.00	0.00	0.00
$C_2H_4 + \dot{C}_2H_3$	1.60	1.48	1.68	1.70
$\dot{C}_4H_7$1-3	5.51	5.69	5.92	–
$\dot{C}_4H_7$1-4	4.86	5.00	5.28	5.55
TS: $C_4H_6 + \dot{H} \rightarrow \dot{C}_4H_7$1-3	0.67	0.60	1.06	0.73
TS: $C_4H_6 + \dot{H} \rightarrow \dot{C}_4H_7$1-4	0.94	0.85	1.26	1.03
TS: $C_2H_4 + \dot{C}_2H_3 \rightarrow \dot{C}_4H_7$1-4	2.72	2.77	3.00	3.06
TS: $\dot{C}_4H_7$1-3 $\rightarrow \dot{C}_4H_7$1-4	2.75	2.78	2.97	2.94

[a] All are relative to that calculated for C_4H_6 + H.

Single Point Energies (SPEs) were calculated using spin-restricted and spin-unrestricted approaches for the open shell species and transition states of the important reaction channels presented in Fig. 1.

- Method 1: CCSD(T)/cc-pVTZ, QZ//M06-2X/6-311++G(d,p)
- Method 2: CCSD(T) and MP2/aug-cc-pVTZ, QZ//wB97XD/aug-cc-pVTZ

The calculated SPEs are compared in Table 9, with all energies relative to the $C_4H_6 + \dot{H}$ reactants. Again, for each approach there is less than 0.4 kcal mol^{-1} difference observed for all species and transition states listed when the same spin treatment is used. However, for each method, when comparing the SPEs calculated using the two different spin treatments, 0.3 – 1.3 kcal mol^{-1} discrepancies are observed. The SPEs calculated using the spin-restricted approach are lower than those using the spin-unrestricted approach.

Table 9: SPEs comparison between two different approaches. (units: kcal mol^{-1}).

	Method 1		Method 2	
Species & Transition States	Spin Restricted	Spin Unrestricted	Spin Restricted	Spin Unrestricted
$C_4H_6 + \dot{H}$	0.00	0.00	0.00	0.00
$C_2H_4 + \dot{C}_2H_3$	3.05	3.34	2.82	3.32
$\dot{C}_4H_7$1-3	–51.14	–50.74	–51.22	–50.62
$\dot{C}_4H_7$1-4	–33.68	–33.67	–33.88	–33.79
TS: $C_4H_6 + \dot{H} \rightarrow \dot{C}_4H_7$1-3	0.83	1.89	0.66	1.94
TS: $C_4H_6 + \dot{H} \rightarrow \dot{C}_4H_7$1-4	3.96	4.94	3.74	5.00
TS: $C_2H_4 + \dot{C}_2H_3 \rightarrow \dot{C}_4H_7$1-4	6.37	7.00	5.95	6.92
TS: $\dot{C}_4H_7$1-3 $\rightarrow \dot{C}_4H_7$1-4	0.80	1.16	0.69	1.24

Table 10 shows the forward and reverse barrier heights using the two different approaches and methods (note, the energy values in this table include both ZPEs and SPEs). The biggest discrepancies are generally for reverse barrier heights in the dissociation reactions, where the spin-unrestricted approach gives about 0.4 – 1.3 kcal mol^{-1} higher barrier than spin-restricted approach.

Table 10: Barrier height comparisons between two different approaches. (units: kcal mol^{-1}).

	Method 1				Method 2			
	Spin Restricted		Spin Unrestricted		Spin Restricted		Spin Unrestricted	
Reactions	Forward	Reverse	Forward	Reverse	Forward	Reverse	Forward	Reverse
$\dot{C}_4H_7$1-3 ↔ C_4H_6 + Ḣ	47.13	1.49	47.80	2.56	46.79	1.26	47.47	2.54
$\dot{C}_4H_7$1-3 ↔ $\dot{C}_4H_7$1-4	49.19	32.38	49.15	32.72	49.00	32.36	48.95	32.81
$\dot{C}_4H_7$1-4 ↔ C_4H_6 + Ḣ	33.72	4.90	34.69	5.88	33.48	4.59	34.64	5.85
$\dot{C}_4H_7$1-4 ↔ C_2H_4 + $\dot{C}_2H_3$	37.91	4.44	38.53	4.79	37.60	4.41	38.48	4.89

The C_4H_6 + Ḣ ↔ products bimolecular reaction has been selected to illustrate the effect of the variation in the SPEs from the two approaches (restricted and unrestricted) on the predicted rate constants. In Fig. 8 black and red lines are the rate constants calculated using the spin-restricted and spin-unrestricted SPE approaches respectively, while solid and dashed lines are the HPL and total rate constants at 0.1 atm, respectively. The spin-unrestricted SPEs approach consistently under-predicts rate constants, particularly at lower temperatures. This can be explained by the predicted higher barriers as mentioned above. Our comparison indicates that the results from the spin-restricted approach agree better with experimental data than the spin-unrestricted calculations.

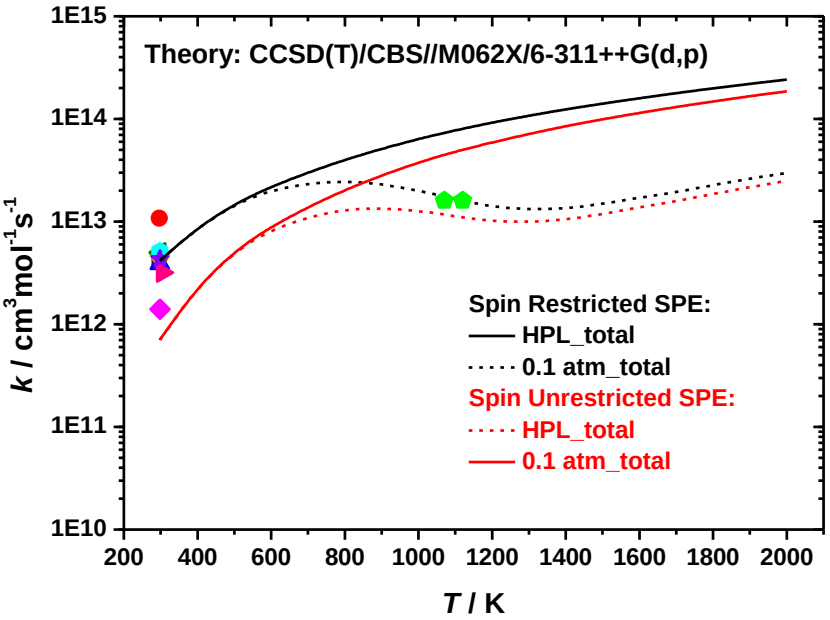

Fig. 8. Spin-restricted and unrestricted SPEs effect on the rate constant calculated for C_4H_6 + Ḣ → products. (Experiments: Jennings *et al.* [53], Yang *et al.* [54], Woolley *et al.* [55], Cvetanovic *et al.* [56], Koda *et al.* [57], Daby *et al.* [58], Gordon *et al.* [59], Ishikawa *et al.* [60], Oka *et al.* [61], Nametkin *et al.* [62])

3.6. Thermochemistry Comparison between Two Different Quantum Chemical Methods and Codes

The thermochemistry of all C_4 species (C_4H_6 and $\dot{C}_4H_7$ isomers) on the PES have been calculated using the two different quantum chemical methods and codes. In order to compare the values calculated, 1,3-butadiene (C_4H_6) and 1-butyne (C_4H_6-1) have been selected as representatives species for which data is also available from two other reliable sources, namely the Active Thermochemical Tables (ATcT)[45-47] and from the bond additivity corrected QCISD(T)/CBS calculations of Goldsmith *et al.*[65] Table 11 compares the 298 K enthalpies of formation and entropies of 1,3-butadiene (C_4H_6) and 1-butyne (C_4H_6-1) calculated here from our two different quantum chemical methods and the values from the literature.

- Method 1: CBS-APNO/G3/G4//M06-2X/6-311++G(d,p)
- Method 2: CBS-APNO/G3/G4//wB97XD/aug-cc-pVTZ
- ATcT: Refs. [45-47]
- Goldsmith: RQCISD(T)/cc-pVT,QZ//B3LYP/6-311++G(d,p), with bond additivity correction

Table 11: Comparison of thermochemical values* from two different quantum chemical methods and from literature data.

Species	$\Delta_f H_{298\,K}$				$S_{298\,K}$			
	Method 1	Method 2	ATcT	Goldsmith	Method 1	Method 2	ATcT	Goldsmith
C_4H_6	26.68	26.64	26.43 ± 0.1	26.50	66.60	66.38	–	65.80
C_4H_6-1	39.79	39.77	39.62 ± 0.2	40.10	69.09	68.98	–	69.20

*Units: kcal mol^{-1} for heat of formation, cal K^{-1} mol^{-1} for entropy.

Excellent agreement was obtained for the values from four different sources, with less than 0.5 kcal mol^{-1} and 0.8 cal K^{-1} mol^{-1} differences in the heats of formation and entropy values, respectively. Such agreement once again confirms the consistency and accuracy of the two methods used in this study. Moreover, from the calculation expense viewpoint, significantly "cheaper" methods can still produce accurate results.

In order to compare thermochemical values calculated by two different codes, the most important C_4 radicals: 1-methylallyl ($\dot{C}_4H_7$1-3) and 3-buten-1-yl ($\dot{C}_4H_7$1-4) radicals have been selected as representatives. Table 12 compares the 298 K enthalpies of formation, entropies and heat capacity as a function of temperature calculated using the two different codes. Again, excellent agreement is obtained over the entire temperature range, with less than 0.02 kcal mol^{-1}, 0.03 cal K^{-1} mol^{-1} and 0.09 cal K^{-1} mol^{-1} differences in the heats of formation, entropy and heat capacity values, respectively.

Table 12: Thermochemical values* comparison between two different codes.

Species	$\dot{C}_4H_7$1-3		$\dot{C}_4H_7$1-4	
	MultiWell/Thermo	PAPR	MultiWell/Thermo	PAPR
$\Delta_f H_{298K}$	31.71	31.71	48.94	48.92
S_{298K}	72.02	72.03	77.23	77.20
Cp_{300K}	19.93	19.90	20.11	20.20

Cp_{400K}	24.92	24.90	24.93	24.98
Cp_{500K}	29.41	29.40	29.23	29.26
Cp_{600K}	33.21	33.20	32.85	32.87
Cp_{800K}	39.17	39.16	38.57	38.58
Cp_{1000K}	43.61	43.60	42.87	42.87
Cp_{1500K}	50.61	50.60	49.72	49.72

*Units: kcal mol^{-1} for heat of formation, cal K^{-1} mol^{-1} for entropy and heat capacity.

3.7. Rate Constants Comparison of H-atom Abstraction by H-Atom

A sensitivity analysis with our recently developed 1,3-butadiene[6] oxidation mechanism indicates that the branching ratio between Ḣ-atom addition and abstraction is critical to predicting flame speeds, Fig. 9.

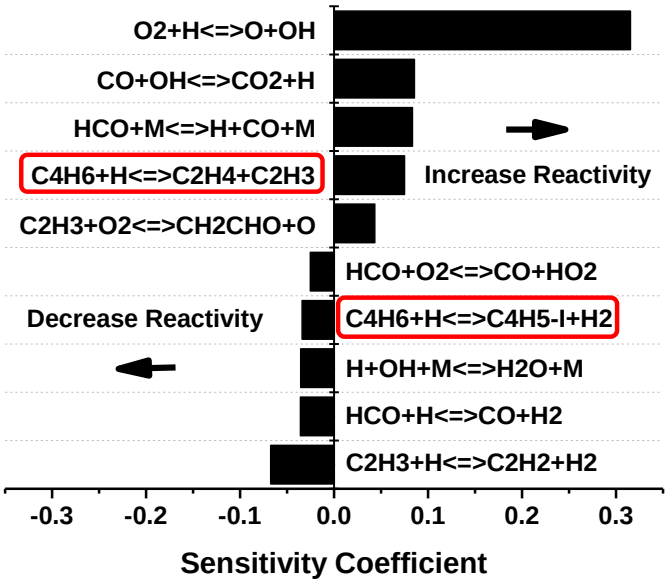

Fig. 9. Flame speed sensitivity analysis of C_4H_6/air laminar flame at φ = 1.1, T_u = 298 K, p = 1 atm.

Thus, the rate constants for H-atom abstraction by Ḣ atoms were calculated with *ab initio* TST using the two different quantum chemical methods and codes discussed above. The predictions are illustrated in Fig. 10, where black and red lines represent rate constants for abstraction of central and terminal H-atoms, respectively, and solid and dashed lines correspond to the values calculated using the two different quantum chemical methods. Throughout the temperature range of 600–2000 K, there is less than 40% difference observed between the results. The branching ratio for abstraction from central and terminal carbon atoms are compared at three selected temperatures: 600, 1300 and 2000 K. Central abstraction dominates over terminal abstraction, which is consistent with the calculated bond dissociation energy (BDE) difference between secondary allylic-vinylic (101.5 kcal mol^{-1}) and primary vinylic (110.53 kcal mol^{-1}) C–H bonds in the 1,3-butadiene molecule.

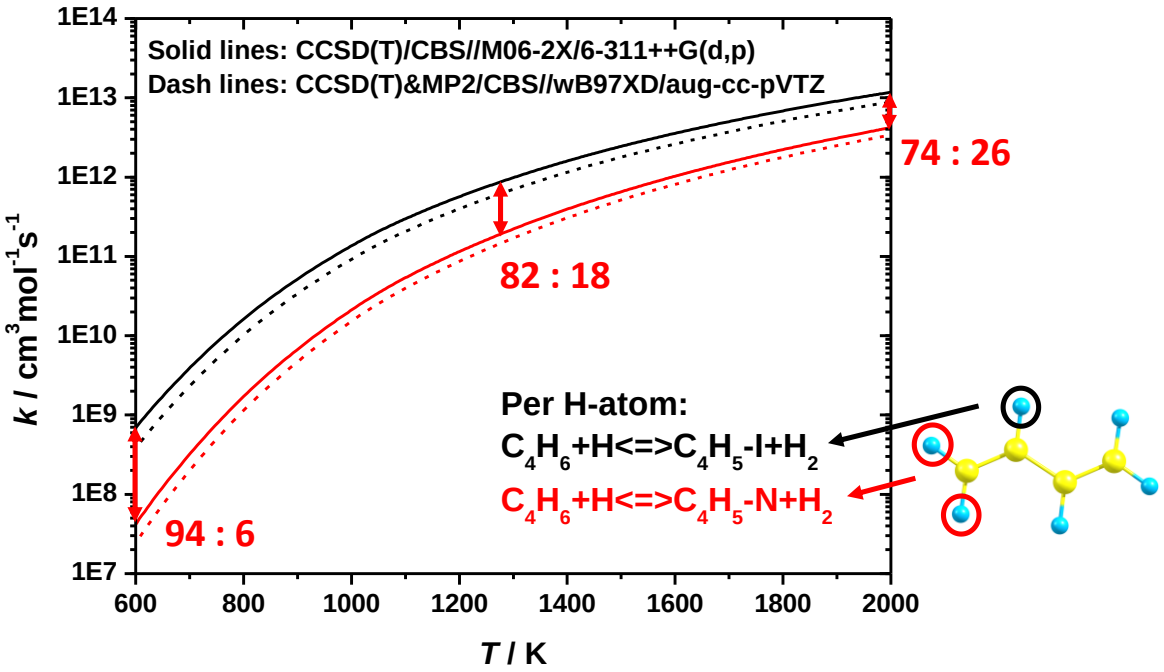

Fig. 10. Rate constants for Ḣ-atom abstraction by Ḣ atoms.

It is worth discussing the $\dot{C}_4H_5$-I free radical formed as a result of abstraction of a H-atom from a central carbon atom. This radical is resonantly stabilized due to the presence of vinylic and allenic structures, Fig. 11. Table 13 shows the enthalpy of formation at 298 K and distribution x_i of these two structures, which is determined from Boltzmann distribution, taking due account of Gibbs free energies $\Delta G^{\ominus}$ and degeneracies σ:

$$x_i = \sigma_i exp(-\Delta G_m^{\Theta}(i)/RT) \sum_{i=1}^{n} [\sigma_i exp(-\Delta G_m^{\Theta}(i)/RT)]$$

This shows that the allenic structure is about 8.5 kcal mol^{-1} more stable than the vinylic one, and thus the allenic structure dominates. In addition, a CASPT2(5e,5o)/cc-pVTZ analysis (with all pi and radical orbitals active) shows that the electronic barrier from the vinylic to the allenic structure is only 0.03 kcal mol^{-1}, and ZPE corrections actually make this value negative. Therefore, we believe that the $\dot{C}_4H_5$-I radical will always exist in the allenic form, and the subsequent reaction pathways should be represented accordingly.

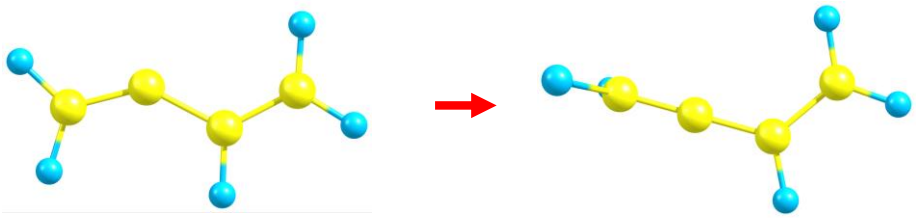

(a) Vinylic Structure (b) Allenic Structure

Fig. 11. Vinylic and allenic resonance structures of the $\dot{C}_4H_5$-I radical.

Table 13 Energies and distribution of vinylic and allenic structured $\dot{C}_4H_5$-I radical.

Name	Vinylic Structure	Allenic Structure
$\Delta_f H_{298K}$ (kcal mol^{-1})	83.50	75.08
Distribution (298 – 2000 K)	≤ 25%	≥ 75%

3.8. Application in Kinetic Model Development

The calculated pressure-dependent rate coefficients of the reactions on the $\dot{C}_4H_7$ PES and H-atom abstraction rate coefficients have been incorporated into our recently developed 1,3-butadiene[6] oxidation mechanism. Laminar flame speed measurements have been selected as the representative target as these are particularly sensitive to $\dot{H}$ atom chemistry, Fig. 12. Herein, the solid lines are the model predictions incorporating the rate coefficients calculated in the current study and the dashed lines represent those using the rate coefficients from AramcoMech2.0.[4] It is clear that using the rate coefficients from the current study leads to improved flame speed predictions. Such improvement reflects on the accurate prediction of the H-atom addition and abstraction branching ratio shown in Fig. 9. A further detailed discussion of its effects on model prediction is beyond the scope of this paper and is provided in Ref. 6.

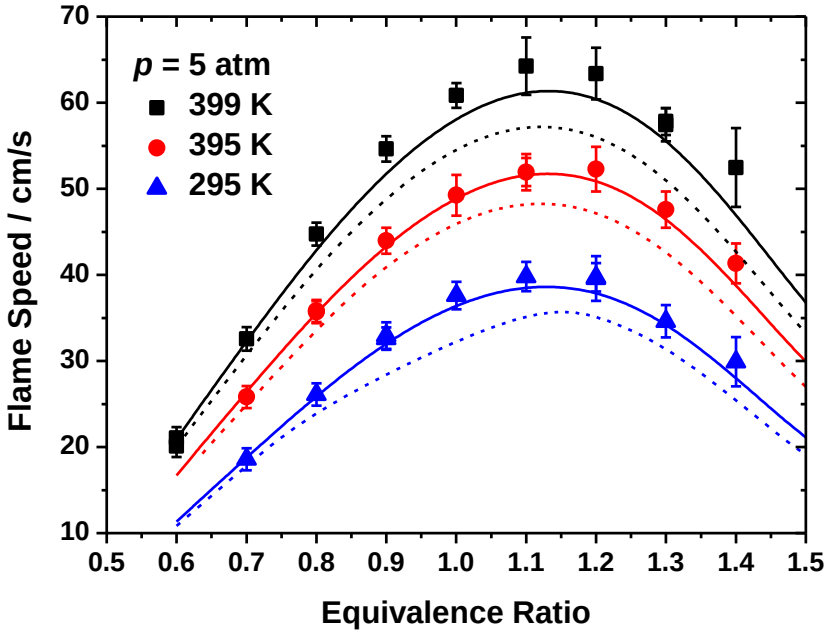

Fig. 12. 1,3-Butadiene laminar flame speed. Solid line: Model prediction incorporating the rate coefficients calculated in the current study; Dashed line: Model prediction with original rate coefficients in AramcoMech2.0.

4. Conclusions

This study provides a wide-ranging theoretical treatment of the kinetics associated with the $\dot{C}_4H_7$ PES. The pressure-dependent rate coefficients for isomerization, decomposition and chemical activation reactions were investigated using RRKM/ME analyses. The thermodynamic properties of all C_4 species were also evaluated. Two entrance channels: 1-methylallyl ($\dot{C}_4H_7$1-3) and 3-buten-1-yl ($\dot{C}_4H_7$1-4) were found to be the most important wells, and production of $C_2H_4 + \dot{C}_2H_3$, which tends to promote reactivity, was found to be the most important bimolecular reaction. Systematic comparisons were made among different quantum chemical methods, approaches, codes and literature data for the various results generated in this study including ZPEs, SPEs, rate constants, barrier heights and thermochemistry.

- ZPEs were compared between four different quantum chemical methods: M06-2X/6-311++G(d,p), wB97XD/aug-cc-pVTZ, B2PLYP-D3/cc-pVTZ and CCSD(T)/cc-pVTZ.

- SPEs were compared between spin-restricted and -unrestricted approaches.
- HPL rate constants and thermochemistry were compared between two different codes: MultiWell/Thermo and PAPR.
- HPL rate constants, barrier heights and thermochemistry were compared between two different quantum chemical methods: CCSD(T)/CBS//M06-2X/6-311++G(d,p) and CCSD(T)&MP2/CBS//wB97XD/aug-cc-pVTZ.
- Pressure-dependent rate constants, barrier heights and thermochemistry were compared against both experimental and theoretical results in literature.

Considering all of the above comparisons, reasonably good agreement was obtained between two different quantum chemical methods and two different codes. Excellent agreement was observed between the theoretical and experimental results available over a wide range of conditions. In addition, the comparison between the two different quantum chemical methods demonstrates that the second method (CCSD(T) and MP2/CBS//wB97XD/aug-cc-pVTZ) is able to approximate a "higher-level" answer at a lower computational cost, hence this method is recommended for the calculation of the pentene + Ḣ and pentadiene + Ḣ reaction systems in the future. Regarding the comparison between spin-restricted and spin-unrestricted approaches for SPEs calculation, it was found that the spin-unrestricted approach tends to over-predict the barrier heights of bimolecular reactions, which results in the under-prediction of rate constants especially at lower temperatures (298 – 1000 K).

Furthermore, the calculated H-atom addition and abstraction rate coefficients were incorporated into a recently developed 1,3-butadiene model. The laminar flame speed simulations clearly demonstrate a significant improvement in model predictions, emphasizing the value of this study.

Supplementary Material

Rate coefficients (for an N_2 bath) have been fitted to the PLOG[49] format, and are provided as a function of temperature by the sum of two modified Arrhenius functions at various pressures. Thermochemical values for all C_4 species are provided at selected temperatures and fitted to ChemKin style NASA polynomials[49] format. In addition, the input files for both MultiWell/Thermo and PAPR codes are also provided.

Acknowledgments

This work is supported by the FUELCOM project of Saudi Aramco and by Science Foundation Ireland via their Principal Investigator Program through project number 15/IA/3177. The work at Argonne was supported by the U.S. Department of Energy, Office of Science, Office of Basic Energy Sciences, Division of Chemical Sciences, Geosciences, and Biosciences under Contract No. DE-AC02-06CH11357. The authors wish to acknowledge the computational resources provided from the Irish Centre for High-End Computing (ICHEC), under project number ngche043c. We also appreciate the provision of automation Perl code from Dr. Kieran Somers, and MESS_TPfit code from Prof. C. Franklin Goldsmith.

References

1. Burke, S. M.; Metcalfe, W.; Herbinet, O.; Battin-Leclerc, F.; Haas, F. M.; Santner, J.; Dryer, F. L.; Curran, H. J., An experimental and modeling study of propene oxidation. Part 1: Speciation measurements in jet-stirred and flow reactors. *Combust. Flame* **2014,** *161* (11), 2765-2784.
2. Burke, S. M.; Burke, U.; Mc Donagh, R.; Mathieu, O.; Osorio, I.; Keesee, C.; Morones, A.; Petersen, E. L.; Wang, W.; DeVerter, T. A.; Oehlschlaeger, M. A.; Rhodes, B.; Hanson, R. K.; Davidson, D. F.; Weber, B. W.; Sung, C.-J.; Santner, J.; Ju, Y.; Haas, F. M.; Dryer, F. L.; Volkov, E. N.; Nilsson, E. J. K.; Konnov, A. A.; Alrefae, M.; Khaled, F.; Farooq, A.; Dirrenberger, P.; Glaude, P.-A.; Battin-Leclerc, F.; Curran, H. J., An experimental and modeling study of propene oxidation. Part 2: Ignition delay time and flame speed measurements. *Combust. Flame* **2015,** *162* (2), 296-314.
3. Li, Y.; Zhou, C.-W.; Curran, H. J., An extensive experimental and modeling study of 1-butene oxidation. *Combustion and Flame* **2017,** *181*, 198-213.
4. Li, Y.; Zhou, C.-W.; Somers, K. P.; Zhang, K.; Curran, H. J., The oxidation of 2-butene: A high pressure ignition delay, kinetic modeling study and reactivity comparison with isobutene and 1-butene. *Proceedings of the Combustion Institute* **2017,** *36* (1), 403-411.
5. Zhou, C.-W.; Li, Y.; O'Connor, E.; Somers, K. P.; Thion, S.; Keesee, C.; Mathieu, O.; Petersen, E. L.; DeVerter, T. A.; Oehlschlaeger, M. A.; Kukkadapu, G.; Sung, C.-J.; Alrefae, M.; Khaled, F.; Farooq, A.; Dirrenberger, P.; Glaude, P.-A.; Battin-Leclerc, F.; Santner, J.; Ju, Y.; Held, T.; Haas, F. M.; Dryer, F. L.; Curran, H. J., A comprehensive experimental and modeling study of isobutene oxidation. *Combust. Flame* **2016,** *167*, 353-379.
6. Zhou, C.-W.; Li, Y.; Burke, U.; Somers, K. P.; Khan, S.; Hargis, J. W.; Sikes, T.; Petersen, E. L.; AlAbbad, M.; Farooq, A.; Pan, Y.; Zhang, Y.; Huang, Z.; Lopez, J.; Loparo, Z.; Vasu, S. S.; Curran, H. J., An Experimental and Chemical Kinetic Modeling Study of 1,3-Butadiene Combustion: Ignition delay time and laminar flame speed measurements, (under review). *Combust. Flame* **2017**.
7. Laskin, A.; Wang, H.; Law, C. K., Detailed kinetic modeling of 1,3-butadiene oxidation at high temperatures. *Int. J. Chem. Kinet.* **2000,** *32* (10), 589-614.
8. Miller, J. L., Theoretical Study of the Straight-Chain C4H7 Radical Isomers and Their Dissociation and Isomerization Transition States. *J. Phys. Chem. A* **2004,** *108* (12), 2268-2277.
9. Miyoshi, A., Computational studies on the reactions of 3-butenyl and 3-butenylperoxy radicals. *Int. J. Chem. Kinet.* **2010,** *42* (5), 273-288.
10. Xu, C.; Al Shoaibi, A. S.; Wang, C.; Carstensen, H.-H.; Dean, A. M., Kinetic Modeling of Ethane Pyrolysis at High Conversion. *J. Phys. Chem. A* **2011,** *115* (38), 10470-10490.
11. Huang, C.; Yang, B.; Zhang, F., Pressure-dependent kinetics on the C4H7 potential energy surface and its effect on combustion model predictions. *Combust. Flame* **2017,** *181*, 100-109.
12. Shestov, A. A.; Popov, K. V.; Slagle, I. R.; Knyazev, V. D., Kinetics of the reaction between vinyl radical and ethylene. *Chem. Phys. Lett.* **2005,** *408* (4–6), 339-343.
13. Ismail, H.; Goldsmith, C. F.; Abel, P. R.; Howe, P.-T.; Fahr, A.; Halpern, J. B.; Jusinski, L. E.; Georgievskii, Y.; Taatjes, C. A.; Green, W. H., Pressure and Temperature Dependence of the Reaction of Vinyl Radical with Ethylene. *J. Phys. Chem. A* **2007,** *111* (29), 6843-6851.
14. Barker, J. R.; Nguyen, T. L.; Stanton, J. F.; C. Aieta, M. C.; Gabas, F.; Kuma, T. J. D.; Li, C. G. L.; Lohr, L. L.; Maranzana, A.; Ortiz, N. F.; Preses, J. M.; Stimac, P. J., MultiWell-2016 Software Suite; J. R. Barker, University of Michigan, Ann Arbor, Michigan, USA. **2016**.
15. Georgievskii, Y.; Miller, J. A.; Burke, M. P.; Klippenstein, S. J., Reformulation and Solution of the Master Equation for Multiple-Well Chemical Reactions. *J. Phys. Chem. A* **2013,** *117* (46), 12146-12154.
16. Foresman, J.; Ortiz, J.; Cioslowski, J.; Fox, D., Gaussian 09, Revision D. 01; Gaussian, Inc. *Wallingford, CT* **2009**.
17. Zhao, Y.; Truhlar, D. G., The M06 suite of density functionals for main group thermochemistry, thermochemical kinetics, noncovalent interactions, excited states, and transition elements: two new functionals and systematic testing of four M06-class functionals and 12 other functionals. *Theor. Chem. Acc.* **2008,** *120* (1), 215-241.
18. McLean, A. D.; Chandler, G. S., Contracted Gaussian basis sets for molecular calculations. I. Second row atoms, Z=11–18. *The Journal of Chemical Physics* **1980,** *72* (10), 5639-5648.
19. Krishnan, R.; Binkley, J. S.; Seeger, R.; Pople, J. A., Self‐consistent molecular orbital methods. XX. A basis set for correlated wave functions. *The Journal of Chemical Physics* **1980,** *72* (1), 650-654.
20. Jr., T. H. D., Gaussian basis sets for use in correlated molecular calculations. I. The atoms boron through neon and hydrogen. *The Journal of Chemical Physics* **1989,** *90* (2), 1007-1023.
21. III, G. D. P.; Bartlett, R. J., A full coupled‐cluster singles and doubles model: The inclusion of disconnected triples. *The Journal of Chemical Physics* **1982,** *76* (4), 1910-1918.
22. Martin, J. M. L., Ab initio total atomization energies of small molecules — towards the basis set limit. *Chem. Phys. Lett.* **1996,** *259* (5), 669-678.
23. Feller, D.; Dixon, D. A., Extended benchmark studies of coupled cluster theory through triple excitations. *The Journal of Chemical Physics* **2001,** *115* (8), 3484-3496.
24. Chai, J.-D.; Head-Gordon, M., Long-range corrected hybrid density functionals with damped atom-atom dispersion corrections. *PCCP* **2008,** *10* (44), 6615-6620.

25. Kendall, R. A.; Jr., T. H. D.; Harrison, R. J., Electron affinities of the first - row atoms revisited. Systematic basis sets and wave functions. *The Journal of Chemical Physics* **1992,** *96* (9), 6796-6806.
26. Woon, D. E.; Jr., T. H. D., Gaussian basis sets for use in correlated molecular calculations. III. The atoms aluminum through argon. *The Journal of Chemical Physics* **1993,** *98* (2), 1358-1371.
27. Head-Gordon, M.; Head-Gordon, T., Analytic MP2 frequencies without fifth-order storage. Theory and application to bifurcated hydrogen bonds in the water hexamer. *Chem. Phys. Lett.* **1994,** *220* (1), 122-128.
28. Hratchian, H. P.; Schlegel, H. B., Using Hessian Updating To Increase the Efficiency of a Hessian Based Predictor-Corrector Reaction Path Following Method. *Journal of Chemical Theory and Computation* **2005,** *1* (1), 61-69.
29. Lee, T. J.; Taylor, P. R., A diagnostic for determining the quality of single-reference electron correlation methods. *Int. J. Quantum Chem* **1989,** *36* (S23), 199-207.
30. Klippenstein, S. J.; Harding, L. B., Kinetics of the H + NCO reaction. *Proc. Combust. Inst.* **2009,** *32* (1), 149-155.
31. Eyring, H., The Activated Complex in Chemical Reactions. *The Journal of Chemical Physics* **1935,** *3* (2), 107-115.
32. Rice, O. K.; Ramsperger, H. C., THEORIES OF UNIMOLECULAR GAS REACTIONS AT LOW PRESSURES. *J. Am. Chem. Soc.* **1927,** *49* (7), 1617-1629.
33. Rice, O. K.; Ramsperger, H. C., THEORIES OF UNIMOLECULAR GAS REACTIONS AT LOW PRESSURES. II. *J. Am. Chem. Soc.* **1928,** *50* (3), 617-620.
34. Kassel, L. S., Studies in Homogeneous Gas Reactions. I. *The Journal of Physical Chemistry* **1927,** *32* (2), 225-242.
35. Marcus, R. A., Unimolecular Dissociations and Free Radical Recombination Reactions. *The Journal of Chemical Physics* **1952,** *20* (3), 359-364.
36. Marcus, R. A.; Rice, O. K., The Kinetics of the Recombination of Methyl Radicals and Iodine Atoms. *The Journal of Physical Chemistry* **1951,** *55* (6), 894-908.
37. Pilling, M. J.; Robertson, S. H., MASTER EQUATION MODELS FOR CHEMICAL REACTIONS OF IMPORTANCE IN COMBUSTION. *Annu. Rev. Phys. Chem.* **2003,** *54* (1), 245-275.
38. Jasper, A. W.; Miller, J. A., Lennard–Jones parameters for combustion and chemical kinetics modeling from full-dimensional intermolecular potentials. *Combust. Flame* **2014,** *161* (1), 101-110.
39. Klippenstein, S. J.; Miller, J. A., The Addition of Hydrogen Atoms to Diacetylene and the Heats of Formation of i-C4H3 and n-C4H3. *J. Phys. Chem. A* **2005,** *109* (19), 4285-4295.
40. Klippenstein, S. J.; Miller, J. A.; Jasper, A. W., Kinetics of Propargyl Radical Dissociation. *J. Phys. Chem. A* **2015,** *119* (28), 7780-7791.
41. Eckart, C., The Penetration of a Potential Barrier by Electrons. *Physical Review* **1930,** *35* (11), 1303-1309.
42. Ochterski, J. W.; Petersson, G. A.; Jr., J. A. M., A complete basis set model chemistry. V. Extensions to six or more heavy atoms. *The Journal of Chemical Physics* **1996,** *104* (7), 2598-2619.
43. Curtiss, L. A.; Raghavachari, K.; Redfern, P. C.; Rassolov, V.; Pople, J. A., Gaussian-3 (G3) theory for molecules containing first and second-row atoms. *The Journal of Chemical Physics* **1998,** *109* (18), 7764-7776.
44. Curtiss, L. A.; Redfern, P. C.; Raghavachari, K., Gaussian-4 theory. *The Journal of Chemical Physics* **2007,** *126* (8), 084108.
45. Simmie, J. M.; Somers, K. P., Benchmarking Compound Methods (CBS-QB3, CBS-APNO, G3, G4, W1BD) against the Active Thermochemical Tables: A Litmus Test for Cost-Effective Molecular Formation Enthalpies. *J. Phys. Chem. A* **2015,** *119* (28), 7235-7246.
46. Somers, K. P.; Simmie, J. M., Benchmarking Compound Methods (CBS-QB3, CBS-APNO, G3, G4, W1BD) against the Active Thermochemical Tables: Formation Enthalpies of Radicals. *J. Phys. Chem. A* **2015,** *119* (33), 8922-8933.
47. Ruscic, B., Uncertainty quantification in thermochemistry, benchmarking electronic structure computations, and Active Thermochemical Tables. *Int. J. Quantum Chem* **2014,** *114* (17), 1097-1101.
48. Gordon, S.; Mcbride, B. J., Computer Program for Calculation of Complex Chemical Equilibrium Compositions, Rocket Performance, Incident and Reflected Shocks, and Chapman-Jouguet Detonations. *NASA STI* **1976**.
49. ANSYS Chemkin-Pro 17.2, ANSYS, Inc.: San Diego. **2016**.
50. Ibuki, T.; Tsuji, A.; Takezaki, Y., Isomerization of chemically activated 1-buten-1-yl and 1-buten-4-yl radicals. *The Journal of Physical Chemistry* **1976,** *80* (1), 8-14.
51. Miller, J. L.; Krisch, M. J.; Butler, L. J.; Shu, J., Dissociation Channels of the 1-Buten-2-yl Radical and Its Photolytic Precursor 2-Bromo-1-butene. *J. Phys. Chem. A* **2005,** *109* (18), 4038-4048.
52. McCunn, L. R.; Krisch, M. J.; Liu, Y.; Butler, L. J.; Shu, J., A Study of the Unimolecular Dissociation of the 2-Buten-2-yl Radical via the 193 nm Photodissociation of 2-Chloro-2-butene. *J. Phys. Chem. A* **2005,** *109* (29), 6430-6439.
53. Jennings, K. R.; Cvetanović, R. J., Relative Rates of Addition of Hydrogen Atoms to Olefines. *The Journal of Chemical Physics* **1961,** *35* (4), 1233-1240.
54. Yang, K., Free Radical Reactions Initiated by Ionizing Radiation. II. Rate Constants for Hydrogen Atom Addition Reactions with Mono-olefins, Butadiene and Benzene. *J. Am. Chem. Soc.* **1962,** *84* (20), 3795-3799.
55. Woolley, G. R.; Cvetanović, R. J., Production of Hydrogen Atoms by Photolysis of H2S and the Rates of Their Addition to Olefins. *The Journal of Chemical Physics* **1969,** *50* (11), 4697-4704.
56. Cvetanović, R. J.; Doyle, L. C., Relative Rates of Reaction of Hydrogen Atoms with Olefins. *The Journal of Chemical Physics* **1969,** *50* (11), 4705-4713.
57. Seiichiro, K.; Tsutomu, H., A Mass Spectrometric Study of the Reaction of Hydrogen Atom with Butadiene. *Bull. Chem. Soc. Jpn.* **1971,** *44* (10), 2888-2888.

58. Niki, H.; Daby, E. E.; Weinstock, B., Mass-spectrometric studies of rate constants for addition reactions of hydrogen and of deuterium atoms with olefins in a discharge-flow system at 300.deg.K. *The Journal of Physical Chemistry* **1971,** *75* (10), 1601-1610.
59. Gordon, E. B.; Ivanov, B. I.; Perminov, A. P.; Balalaev, V. E., A measurement of formation rates and lifetimes of intermediate complexes in reversible chemical reactions involving hydrogen atoms. *Chem. Phys.* **1978,** *35* (1), 79-89.
60. Yo-ichi, I.; Ko-ichi, S.; Shin, S., The Rate Constants for H and D-Atom Additions to O2, NO, Acetylene, and 1,3-Butadiene. *Bull. Chem. Soc. Jpn.* **1979,** *52* (12), 3503-3506.
61. Oka, K.; Cvetanović, R. J., Determination of rates of hydrogen atom reactions with alkenes at 298 K by a double modulation technique. *Can. J. Chem.* **1979,** *57* (7), 777-784.
62. Nametkin, N. S.; Shevel'kova, L. V.; Kalinenko, R. A., Rate Constants of the Reactions of Hydrogen Atoms with Ethylene and Butadiene at High Temperatures. *Dokl. Chem.* **1975,** *221*, 851.
63. Fahr, A.; Stein, S. E., Reactions of vinyl and phenyl radicals with ethyne, ethene and benzene. *Symposium (International) on Combustion* **1989,** *22* (1), 1023-1029.
64. Klippenstein, S. J., From theoretical reaction dynamics to chemical modeling of combustion. *Proc. Combust. Inst.* **2017,** *36* (1), 77-111.
65. Goldsmith, C. F.; Magoon, G. R.; Green, W. H., Database of Small Molecule Thermochemistry for Combustion. *J. Phys. Chem. A* **2012,** *116* (36), 9033-9057.

TOC Graphic

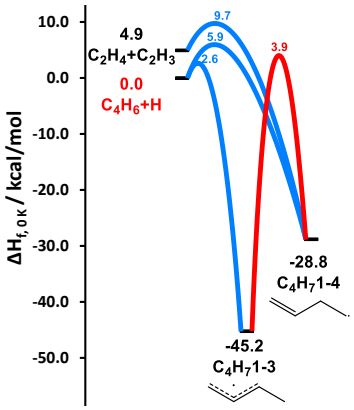
10.0
0.0
-10.0
-20.0
-30.0
-40.0
-50.0
ΔH f, 0 K / kcal/mol
4.9
C2H4+C2H3
0.0
C4H6+H
9.7
5.9
2.6
3.9
-28.8
C4H71-4
-45.2
C4H71-3